buildings

MDPI

Article

A Study of the Shear Behavior of Concrete Beams with Synthetic Fibers Reinforced with Glass and Basalt Fiber-Reinforced Polymer Bars

Isabela Oliveira Duarte, Nadia Cazarim da Silva Forti *, Lia Lorena Pimentel and Ana Elisabete Paganelli Guimarães de Avila Jacintho

Polytechnic School, Pontifical Catholic University of Campinas, Campinas 13086-099, Brazil; isabeladuarte31@hotmail.com (I.O.D.); lialp@puc-campinas.edu.br (L.L.P.); anajacintho@puc-campinas.edu.br (A.E.P.G.d.A.J.)

* Correspondence: nadia.cazarim@puc-campinas.edu.br

Abstract: The use of synthetic materials with high corrosion resistance in a concrete matrix yields structures that are more durable and suitable for use in aggressive environments, eliminating the need for frequent maintenance. Examples of such materials include glass (GFRP) and basalt (BFRP) fiber-reinforced polymer bars (FRP). Due to the low modulus of elasticity of these bars, concrete elements reinforced with FRP longitudinal rebars tend to exhibit cracks with wider openings and greater depths compared to those reinforced with steel rebars, which diminishes the element's shear resistance. The addition of discontinuous fibers into the concrete aims to maintain stress transfer across the cracks, thereby enhancing the shear capacity and ductility of FRP-reinforced structures. This study evaluates the impact of fiber addition on the shear resistance of concrete beams reinforced with FRP rebars. An experimental investigation was conducted, focusing on the partial and complete substitution of stirrups with polypropylene macro fibers in concrete beams reinforced with FRP longitudinal rebars and stirrups. This research examined beams reinforced with glass (GFRP) and basalt (BFRP) fiber-reinforced polymer bars. For the initial set of beams, all stirrups were replaced with synthetic macro fibers. In the subsequent set, macro fibers were added to beams with insufficient stirrups. Although the complete replacement of GFRP and BFRP stirrups with polypropylene macro fibers did not alter the brittle shear failure mode, it did enhance the shear resistance capacity by 78.5% for GFRP-reinforced beams and 60.4% for BFRP-reinforced beams. Furthermore, the addition of macro fibers to beams with insufficient stirrups, characterized by excessive spacing, changed the failure mode from brittle shear to pseudo-ductile flexural failure due to concrete crushing. In such instances, the failure load increased by 18.8% for beams with GFRP bars and 22.8% for beams with BFRP bars.

Keywords: concrete structures; BFRP bars; GFRP bars; fiber-reinforced concrete; shear behavior

check for updates

Citation: Duarte, I.O.; Forti, N.C.d.S.; Pimentel, L.L.; Jacintho, A.E.P.G.d.A. A Study of the Shear Behavior of Concrete Beams with Synthetic Fibers Reinforced with Glass and Basalt Fiber-Reinforced Polymer Bars. *Buildings* **2024**, *14*, 2123. https://doi.org/10.3390/buildings14072123

Academic Editor: Chenggao Li

Received: 17 May 2024
Revised: 26 June 2024
Accepted: 3 July 2024
Published: 11 July 2024

Copyright: © 2024 by the authors. Licensee MDPI, Basel, Switzerland. This article is an open access article distributed under the terms and conditions of the Creative Commons Attribution (CC BY) license (https://creativecommons.org/licenses/by/4.0/).

1. Introduction

The construction sector has a great influence on the economic and social development of a country, but it still stands out as a major generator of environmental impacts. Due to the growing concern about the negative interferences that this sector causes in the environment, new alternatives are developed seeking to promote more durable structures that consume fewer natural resources and generate less waste. The use of fiber-reinforced polymer bars is an example of a technique that has been studied to promote greater durability in reinforced concrete structures. In addition to having greater resistance to aggressive environments, because they do not suffer corrosion [1–3], they provide longer service life to the structures and provide a reduction in maintenance costs and consequently lower waste generation. Also, the use of corrosion-resistant bars allows for countries with a shortage of fresh water to directly use seawater [2].

Developing countries need investments in infrastructure. The construction of bridges, dams, roads, and marine structures with more efficient and durable materials contributes to social and economic development with less environmental impact.

FRP bars are composed of continuous fibers involved in a polymer matrix. The fibers most used in FRP composites for civil construction are glass fibers (GFRP), carbon, aramid, and more recently, basalt fibers (BFRP). Among the main characteristics of FRP bars are the high resistance/weight ratio, low thermal conductivity, and the fact that they do not suffer corrosion. In addition, because they are composed of non-conductive fibers and have good electrical and magnetic insulation, FRP bars stand out in places subject to the action of magnetic fields, such as hospitals and any environment with sensitive electrical appliances [4].

However, FRP bars do not present plastic behavior. In tensile tests, they fail without warning, showing linear elastic behavior until rupture. In addition, due to the low Young's modulus of FRP bars, structural elements of reinforced concrete with FRP rebars present cracks with greater openings and depth than steel-reinforced structures. Deep fissures decrease the contribution of concrete to shear strength [5].

Studies using GFRP stirrups have pointed to the formation of large diagonal cracks, with a consequent significant loss of interlock between aggregates before the full capacity of the stirrups is reached [6,7]. Moreover, the fibers exhibit wrinkling in the bent zones of the stirrups, leading to premature failure of these components [8]. Therefore, a study is necessary for a better understanding of the shear force transfer mechanisms and how they can be improved [5].

The behavior of concrete beams with FRP bars under flexion has been investigated by many authors, and various approaches have been proposed to assess aspects such as deflection, cracking, stiffness, and strength [9,10]. As previously mentioned, some of the service behavior and ductility issues of these elements can be improved by adding discrete fibers to the matrix.

The addition of discontinuous fibers is an alternative to increase the shear capacity and ductility of concrete structures reinforced with FRP rebars [11]. Discrete fibers are dispersed in concrete and allow tensile stresses to be transferred across cracks [11–13]. The addition of fiber can be used for partial or total replacement of stirrups, steel meshes in slabs, or sprayed concrete panels. They help increase impact resistance and prevent spalling [14,15]. When combined with conventional reinforcement, the fibers help to improve the rebar's adherence strength through confinement action, contributing to the reduction in spacing and crack openings in structural elements [16].

Several studies were conducted to assess the contribution of the addition of discontinuous fibers in the shear behavior of beams reinforced with FRP rebars. The research conducted by Awadallah et al. [11] studied the shear behavior of concrete beams reinforced with steel fibers and reinforced with longitudinal bars of BFRP, with and without steel stirrups. The variables analyzed were steel fiber content (V_f = 0.3%, 0.6%, and 1.2%) with and without minimum shear reinforcement. The experimental study showed that the addition of steel fibers reduced cracking, improved the final shear resistance and ductility of the tested beams, and altered the mode of rupture of the beams for a more ductile behavior. The addition of 0.6% steel fiber increased the load capacity of the beams by 37.5%, while the increase in the addition of 0.6% to 1.2% increased the load capacity of the beams by 18%.

Muhammad and Yousif [12] investigated the impact of basalt macro fiber addition on the shear strength and behavior of concrete beams reinforced longitudinally with basalt FRP bars. Their findings revealed that incorporating macro fibers into FRP-reinforced concrete beams significantly improved the shear strength for both beams with and without stirrups. Notably, the beam with 1.5% BMF exhibited greater shear resistance than the beam with the minimum required BFRP stirrups. Additionally, the post-cracking stiffness of all beams was substantially enhanced following the addition of BMF.

Dev et al. [13] analyzed the effect of the addition of polyolefin synthetic macro fiber (PO) and a hybrid combination of steel and PO fibers on the shear behavior of concrete

beams reinforced with longitudinal GFRP bars. The results indicated that both synthetic and hybrid fibers improved shear resistance and post-cracking behavior, and promoted pseudo-ductility to beams reinforced with GFRP. Hybrid fibers were more efficient in improving overall performance in terms of post-cracking stiffness, residual tensile strength in flexion, and energy absorption. However, this trend was observed only for beams with high fiber dosages of 1% in concrete volume. At a low fiber content (0.35%), although ductility and energy absorption increased, no increase in shear strength was observed due to the addition of fibers.

Thus, this work aims to assess the impact of macro fiber addition on the shear resistance of concrete beams reinforced with FRP rebars. The work focuses on glass (GFRP) and basalt (BFRP) fiber-reinforced polymer bars. In order to achieve the objectives, this study proposes to analyze, through experimental tests, the partial and total replacement of shear reinforcement by adding synthetic fibers in concrete beams reinforced with polymer bars reinforced with glass (GFRP) and basalt (BFRP) fibers. The addition of fibers to the concrete matrix aims to reduce concrete cracking, thus contributing to shear resistance. The goal of adding macro fibers is to maintain stress transfer along cracks and to enhance shear capacity and ductility in structures with FRP rebars.

Section 2 presents the experimental program and characterization of materials. It explains the experimental setup and data acquisition. Digital image correlation is used to measure crack openings. Section 3 brings the results and discusses them. Section 3.3 compares the experimental results with the design procedures of ACI 440.1R-15 [17] and Fib 2010 [18]. Section 4 concludes the article.

2. Materials and Experimental Program

In this work, the partial and total replacement of the shear reinforcement by synthetic macro fiber was evaluated in concrete beams reinforced with GFRP and BFRP rebars. The beams were tested in four-point bending tests.

In total, 8 beams were cast; 4 beams were reinforced with GFRP rebars, and 4 beams were reinforced with BFRP bars. For each type of FRP, the following configurations were tested: Two beams were cast with insufficient stirrups. One was cast with concrete with macro fibers and the other with plain concrete. Two beams were cast with no stirrups: one with fiber-reinforced concrete and the other with plain concrete.

The addition of 1% of the synthetic macro fiber in concrete volume aims to reduce concrete cracking and thus contribute to the shear strength of the structural element. The design of the beams followed the guidelines of ACI 440.1R-15 [17].

2.1. Characterization of Materials

The characterization and selection of the aggregates were carried out according to Brazilian standards [19–21]. The sand's characteristic properties are a maximum dimension of 2.36 mm, modulus of fineness of 1.88, and density of 2.61 g/cm^3. The coarse aggregate has a maximum characteristic size of 19 mm, modulus of fineness of 6.99, and density of 2.82 g/cm^3. The particle size distribution curves of sand and coarse aggregate are shown in Figure 1.

The concrete was mixed with 400 kg/m^3 of Portland cement, 809 kg/m^3 of fine aggregate (sand), 1000 kg/m^3 of coarse aggregate, and 200 kg/m^3 of water. Polycarboxylate-based superplasticizer with a density of 1.040–1.060 kg/m^3 was added (dosage of 1.2 kg/m^3) to avoid the loss of workability and segregation of concrete in the mixes with fiber addition. A polypropylene macro fiber was used. The fibers are classified by EN 14889-2 [22] as Class II, with a density of 0.91 g/cm^3, length of 54 mm, and tensile strength of 550 MPa.

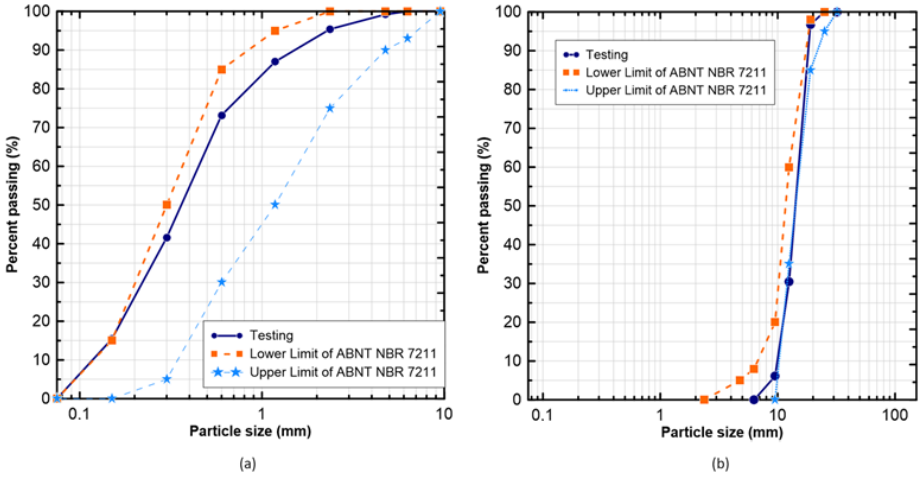

Figure 1. Sand (**a**) and coarse aggregate (**b**) particle size distribution.

The tests performed for the characterization of concrete and their results are presented in Table 1. The concretes have the same dosage and materials but from different batches. Five specimens were cast for each characterization test shown in Table 1. The coefficient of variation (CV) is indicated for each property. An analysis of variance (ANOVA) indicated that the addition of macro fibers caused a reduction in concrete compressive strength. A reduction in Young's modulus is also observed. The tensile strength was not significantly affected. It can be noted that the concrete mixes with fibers present a higher consistency, which is expected. The same dosage of plasticizer was used, and the consistency was adequate to mold the beams.

Table 1. Characterization of plain and fiber-reinforced concrete.

Norm	Essay	Test Results			
		Plain Concrete GFRP	**Fiber-Reinforced Concrete GFRP**	**Plain Concrete BFRP**	**Fiber-Reinforced Concrete BFRP**
NBR 16889/2020 [23]	Consistency by cone trunk abatement (mm)	180	140	200	140
NBR 5739/2018 [24]	Concrete compressive strength (MPa)	49.20	45.25	42.37	36.39
	CV (%)	2.75	10.08	10.47	10.22
NBR 12142/2010 [25]	Tensile strength in bending (MPa)	5.83	5.60	5.93	5.64
	CV (%)	11.75	20.64	8.25	7.13
NBR 8522/2017 [26]	Young's Modulus of concrete (GPa)	34.22	30.98	32.72	30.59
	CV (%)	1.90	4.53	4.49	3.75

Table 2 presents the results of flexural tensile strengths for the fiber-reinforced concretes. The table summarizes the residual strength values obtained at the age of 28 days, according to ABNT NBR 16940 [27] and Fib 2010 [18]. It can be observed that due to the addition of fibers, there was a significant increase in the post-cracking tensile strengths. The fibers provided sufficient residual tensile strength for the concrete to meet the requirements of the Fib 2010 [18] standard for use as a substitute (also partially) for conventional reinforcement in concrete structures ($f_{R1k}/f_{Lk} > 0.40$ and $f_{R3k}/f_{R1k} > 0.50$).

Table 2. Concrete residual strengths.

Concrete for Beams with GFRP							
	f_L	f_{R1}	f_{R2}	f_{R3}	f_{R4}	f_{R1}/f_L	f_{R3}/f_{R1}
Average (MPa)	5.37	3.21	4.09	4.41	4.48	0.60	1.38
Standard Deviation (MPa)	0.32	0.27	0.38	0.34	0.33		
CV (%)	6.00	8.52	9.40	7.59	7.38		
Concrete for Beams with BFRP							
	f_L	f_{R1}	f_{R2}	f_{R3}	f_{R4}	f_{R1}/f_L	f_{R3}/f_{R1}
Average (MPa)	4.40	2.86	3.50	3.64	3.48	0.65	1.27
Standard Deviation (MPa)	0.36	0.28	0.54	0.46	0.41		
CV (%)	8.15	9.68	15.39	12.62	11.85		

The GFRP and BFRP rebars were characterized. Tests of tensile strength and Young's modulus were performed following the procedures of ASTM D7205/D7205M-06 [28]. The results are presented in Table 3. It can be observed that the mechanical behavior (strength and Young's modulus) is very similar for both materials and diameters analyzed.

Table 3. The results of the characterization of the GFRP and BFRP bars.

Material	Nominal Diameter (mm)	Effective Diameter (mm)	Average Tensile Strength (MPa)	Modulus of Elasticity (GPa)
GFRP	6.0	6.44	1033	52
	8.0	7.60	1086	53
	10.0	10.50	997	52
BFRP	6.0	6.50	1039	52
	8.0	7.80	1014	52
	10.0	10.10	1013	53

2.2. Partial and Total Replacement of Shear Reinforcement by Fibers in Concrete Beams Reinforced with GFRP and BFRP Bars

For the identification of the reinforced beams tested, a nomenclature was created in which the material of the longitudinal and transverse reinforcement (GFRP and BFRP), the type of concrete (with and without fiber addition), and the presence (S) or absence (WS) of the stirrups are indicated. For example, GFRP-F-WS stands for a beam reinforced with GFRP rebars, fiber-reinforced concrete, and without stirrups.

The design of the beams reinforced with GFRP or BFRP rebars was performed from the beam dimensions, concrete strength class (estimated at 40 MPa), and the arrangement of longitudinal reinforcement, consisting of five rebars of 10 mm in diameter as shown in Figure 2. The reinforcement arrangement was verified using the procedures of ACI 440.1R-15 standard [17]. The properties were considered as characteristic values, i.e., the properties were adopted without any reduction factor. Then, two values of nominal moment resistance were found (one for each rebar material—GFRP and BFRP), and from them, two values of nominal shear resistance.

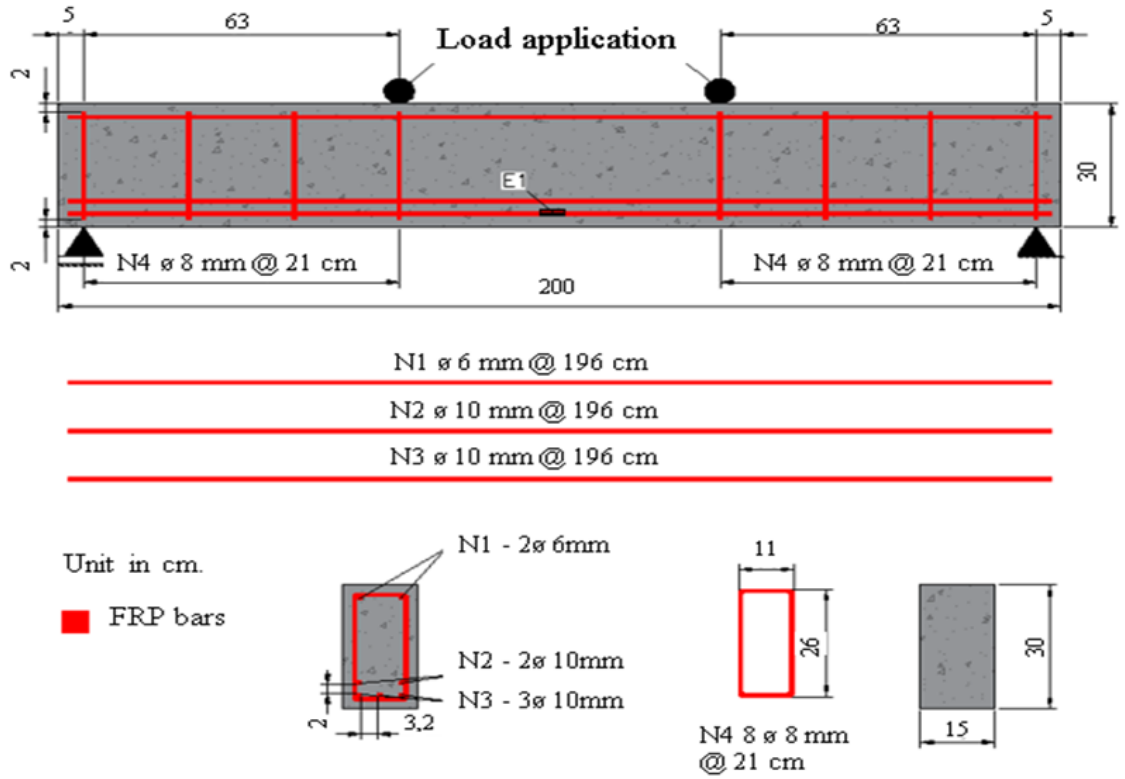

Figure 2. Detailing reinforcement with GFRP and BFRP stirrups.

The following configurations were tested, in a total of eight beams:

- Four beams reinforced with GFRP rebars:
  - Two beams with stirrups with excessive spacing (Figure 2). Macro fibers were added to one beam (labeled GFRP-F-S), and the other beam did not have the addition of fibers (GFRP-WF-S).
  - Two beams without any stirrup. Macro fibers were added to one beam (GFRP-F-WS), and the other beam did not have the addition of fibers (GFRP-WF-WS).
- Four beams reinforced with BFRP rebars:
  - Two beams with stirrups with excessive spacing (Figure 2). Macro fibers were added to one beam (labeled BFRP-F-S), and the other beam did not have the addition of fibers (BFRP-WF-S).
  - Two beams without any stirrup. Macro fibers were added to one beam (BFRP-F-WS), and the other beam did not have the addition of fibers (BFRP-WF-WS).

For the definition of insufficient shear reinforcement, the nominal shear strengths found were considered as the requested shear strength, and, from them, the respective maximum spacing between stirrups was obtained. Then, the spacing of stirrups was determined to induce the rupture by shear of the beam, as shown in Table 4.

The beams have a cross section of 15 cm by 30 cm, a length of 200 cm, and a free span of 190 cm, and both concentrated loads are applied to 63 cm of each support (see Figure 2). The relation between the useful height of the beams and the shear span (a/d) used was approximately 2.5 to induce rupture by shear.

Figure 2 shows the configurations of the reinforcements with stirrups. The beams without stirrups have the same longitudinal rebar configuration shown in Figure 2.

Table 4. Design of beams according to ACI 440.1R-15 [17].

ID	A_{fv}/s_{adot} (cm²/cm)	ACI 440.1R-15 [17]		
		V_U (kN)	S_{max} (cm)	$(A_{fv}/s_{adot})/(A_{fv}/s)$
GFRP-WF-WS	-	82.20	7.49	-
GFRP-WF-S	0.043	82.20	7.49	0.36
GFRP-F-WS	-	82.20	7.49	-
GFRP-F-S	0.043	82.20	7.49	0.36
BFRP-WF-WS	-	80.34	7.86	-
BFRP-WF-S	0.046	80.34	7.86	0.38
BFRP-F-WS	-	80.34	7.86	-
BFRP-F-S	0.046	80.34	7.86	0.38

A_{fv}/s_{adot} = the transverse reinforcement area per unit length of the structural element for shear resistance adopted for the beams; V_U = the factored shear force at the section; S_{max} = the maximum permissible center-to-center bar spacing for flexural crack control; A_{fv}/s = the amount of FRP shear reinforcement within spacing s.

2.3. Bending Tests

The 4-point bending tests were conducted on a gantry with a load capacity of 50 tons. The displacement transducer used to measure the deflection is the WA-50mm-T model, and the Quantum X (DAQ) data acquisition system from HBM was used to read the load and displacement. The test scheme is presented in Figure 3, where the positioning of the beam and the instrumentation used are observed.

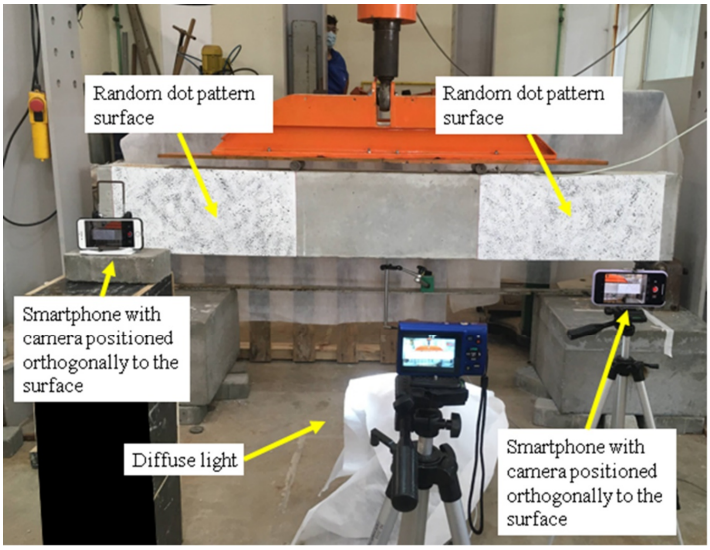

(a)

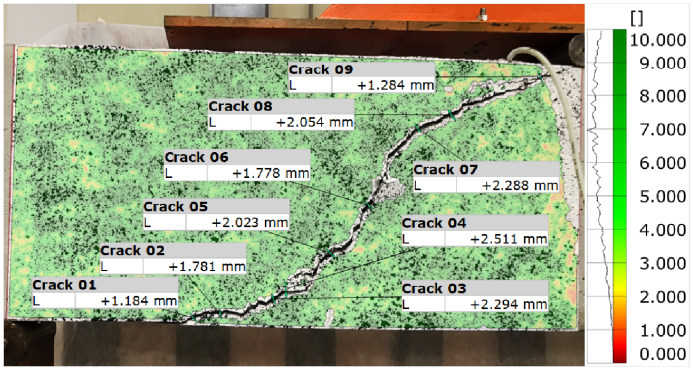

(b)

Figure 3. The setup of the test and positioning of the equipment for application of the DIC technique (**a**). The crack opening readings of BFRP-WF-WS (**b**).

2.4. Digital Image Correlation

Digital image correlation (DIC) involves establishing a relationship between the subsets of pixels from the reference image and the other photos taken during a test. The result of the displacement of a subset corresponds to the average of the displacements of the pixels of this subset, expressed at its center. The step is the distance, in pixels, between the center of a subset of the reference image and the subset of the consecutive image [29]. The pattern of black dots (speckles) was executed aiming to achieve a grayscale, covering 50% of the white surface (Figure 3a). The randomness of the speckles ensures that each pixel subset is unique, enhancing the accuracy of the results derived from the technique [30]. From the surface image at the test start point (reference image), and from the image to a given loading and deformation situation of interest, the comparison between the images, analyzing the change in positioning of the set of points, determines the field of displacement and deformation in the desired region [29]. DIC can be used to measure displacements, longitudinal and shear [31] strains, and crack openings [29].

In this work, the DIC technique was used to measure the opening of the cracks in the tested beams. The beams have been designed to fail by shear, thus the region of interest corresponds to the surfaces delimited by the load points and the supports, i.e., two surfaces of 30 cm × 63 cm as shown in Figure 3a.

The images were recorded using conventional cell phones with 12 megapixels (4032 × 3024 pixels) of resolution, and a 0.156 mm/pixels ratio was adopted for the DIC analysis. Figure 3b shows the crack opening readings of BFRP-WF-WS. The color scale in the figure indicates the quality of the acquired image (10 is the best value). To control the capture speed of the photos, the Lens Buddy application was used, and the capture interval between the photos was defined as 5 s. Gom Correlate V2.0.1 [32] software was used to perform the image correlation analysis. Figure 3b illustrates the measurement of the crack opening.

3. Results and Discussion

Table 5 summarizes the results of the tests of the beams reinforced with GFRP and BFRP rebars.

Table 5. The test results of the beams reinforced with GFRP and BFRP rebars.

ID	A_{fv}/s (cm^2/cm)	Ultimate Load (kN)	V_U Experimental (kN)	Maximum Mid-Span Deflection (mm)	Crack Opening at Failure (mm)	Failure Mode Observed
GFRP-WF-WS	-	70.23	35.11	10.66	1.216	Shear—diagonal failure
GFRP-WF-S	0.043	167.50	83.75	29.84	1.708	Shear—stirrup rupture
GFRP-F-WS	-	125.39	62.68	18.89	2.324	Shear—diagonal failure
GFRP-F-S	0.043	198.92	99.46	35.95	1.609	Concrete crushing bending
BFRP-WF-WS	-	66.08	33.04	13.25	2.511	Shear—diagonal failure
BFRP-WF-S	0.046	145.10	72.55	33.42	2.850	Shear—stirrup rupture
BFRP-F-WS	-	105.98	52.99	17.20	2.940	Shear—diagonal failure
BFRP-F-S	0.046	178.19	89.10	43.58	2.115	Concrete crushing bending

A_{fv}/s = amount of FRP shear reinforcement within spacing s; V_U = factored shear force at section.

Comparing the ultimate load between the beams without stirrups, it can be noted that the beam with fiber-reinforced concrete GFRP-F-WS showed a load capacity (125.39 kN) 78.5% higher than the beam with plain concrete GFRP-WF-WS (70.23 kN). The beam BFRP-F-WS presented a load capacity (105.98 kN) 60.4% higher than BFRP-WF-WS (66.08 kN). Thus, it is clear the contribution of fibers in the shear strength. It can be observed in Table 5 that the beams that failed by shear and had fibers added exhibit larger crack openings at the moment of beam failure, but they can support a much greater load compared to their

counterpart beams without fibers, demonstrating the capacity for load transfer, even after the initiation of cracking.

Comparing the ultimate load between the beams with stirrups, it can be noted that the beam with fiber-reinforced concrete GFRP-F-S showed a load capacity (198.92 kN) 18.8% higher than the beam with plain concrete GFRP-WF-S (167.50 kN). The beam BFRP-F-S showed a load capacity (178.19 kN) 22.8% higher than BFRP-WF-S (145.10 kN). The contribution of fibers is clear, but it is less important than the contribution observed for the beams without stirrups. However, it is important to observe that GFRP-F-S and BFRP-F-S did not fail by shear failure, but in concrete crushing in the bending region. Therefore, the fiber contribution in shear strength could not be fully assessed due to the premature collapse in bending.

Figure 4 compares the failure modes of the tested beams. Beams reinforced with BFRP rebars presented the same behavior as beams reinforced with GFRP bars. When compared to beams without stirrups, with and without the addition of fibers, it is observed that the addition of fibers was not enough to alter the mode of brittle rupture by shear. In FRP-reinforced concrete beams with no stirrups, the applied shear force is carried by the aggregate interlock, dowel effect, and uncracked concrete compression zone, with the formation of a diagonal crack [5]. The lower stiffness of FRP flexural rebars allows the formation of wider shear cracks and weakens aggregate interlock [6].



Figure 4. *Cont.*

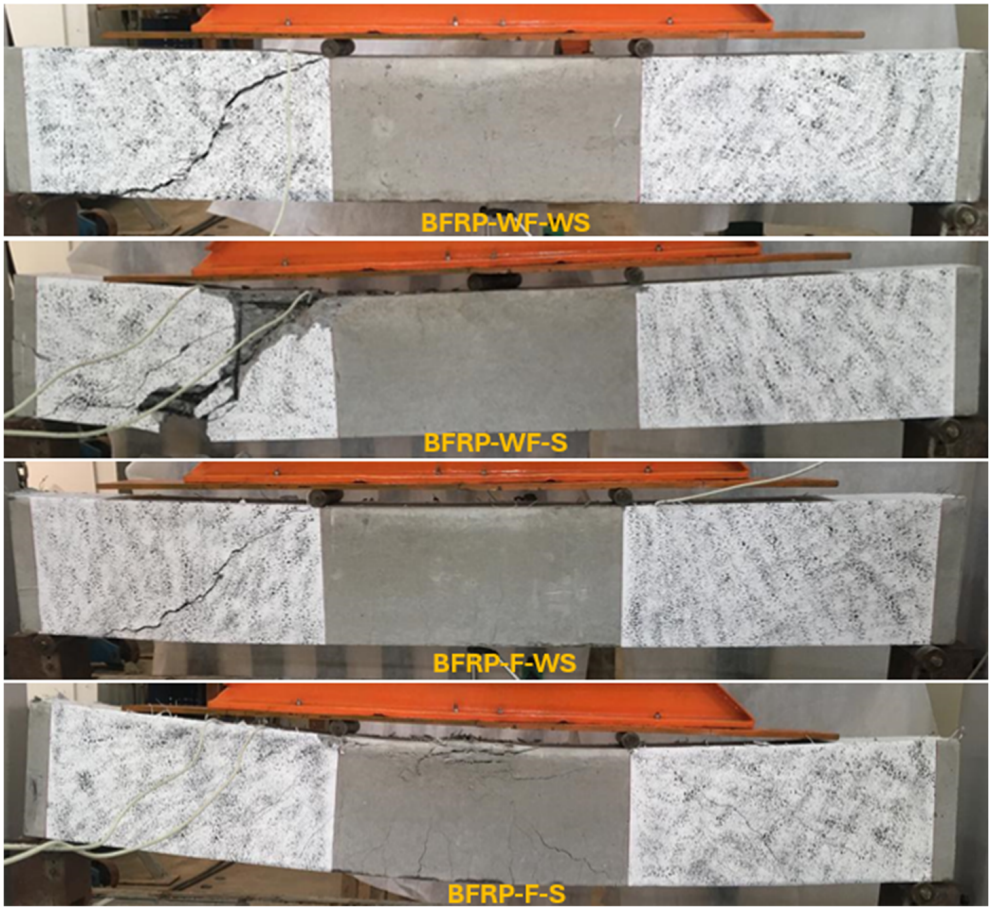

Figure 4. A comparison of the failure modes of the different beam configurations.

On the other hand, when comparing the beams with stirrups, with and without the addition of fibers, it is possible to identify the effect of the fibers on the change in the failure mode. The combination of macro fibers with the stirrups changed the failure mode from brittle shear failure to pseudo-ductile flexural failure due to concrete crushing.

Figure 5 plots the load versus mid-span deflection curves of the beams reinforced with GFRP and BFRP bars.

The beams reinforced without stirrups showed a bilinear behavior until rupture. It is similar to that observed by Said et al. [33]. This bilinear behavior is the result of the mechanical properties of FRP bars, which exhibit linear elastic behavior until their rupture when subjected to tensile stresses.

The beams with stirrups (GFRP-WF-S, BFRP-WF-S, GFRP-F-S, and BFRP-F-S) presented a trilinear behavior. The fibers and stirrups provided greater ductility to the beams and extended the second linear stretch of the deformation curve. It is more pronounced in the beams with the addition of fibers to the concrete.

The beams were cast with the same concrete mix but from different batches. Therefore, their compressive strength varied. In order to better compare the results and mitigate the influence of the different compressive strengths, the shear loads obtained from the experimental tests were normalized according to Equation (1), used by Tomlinson and Fam [34]:

$$\frac{V}{bd\sqrt{f_{c,m}}} \quad (1)$$

where V is the shear load, b is the beam width, d is the depth to flexural reinforcement of the section, and $f_{c,m}$ is the average compressive strength of the concrete. Table 6 presents the results of normalized shear strength for the tested beams. and Figure 6 presents the curves of normalized shear load versus mid-span deflection. It is possible to observe that

the beams reinforced with GFRP and BFRP bars have very similar behaviors throughout the test. The fiber-reinforced concrete beams still collapsed in the shear but with a higher load capacity. Regardless of the type of FRP bar used, after stage I, the beams with stirrups and fibers show a gain in stiffness and load capacity.

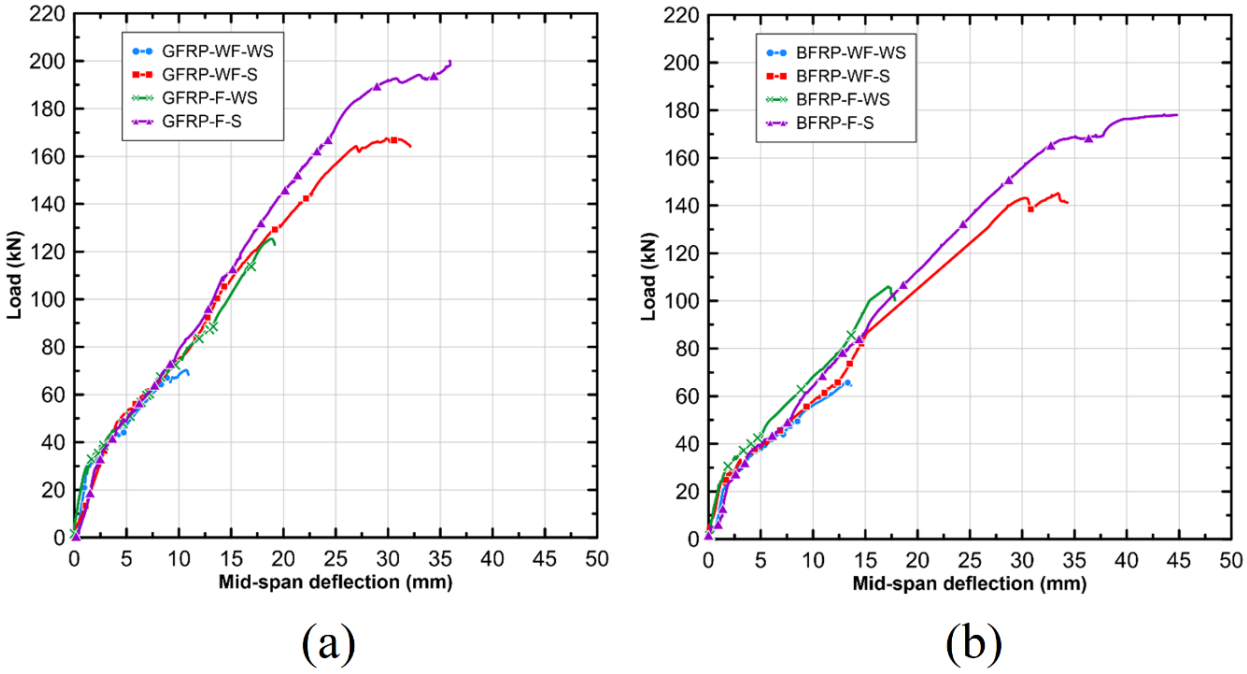

Figure 5. Load × mid-span deflection of beams reinforced with GFRP (**a**) and BFRP (**b**).

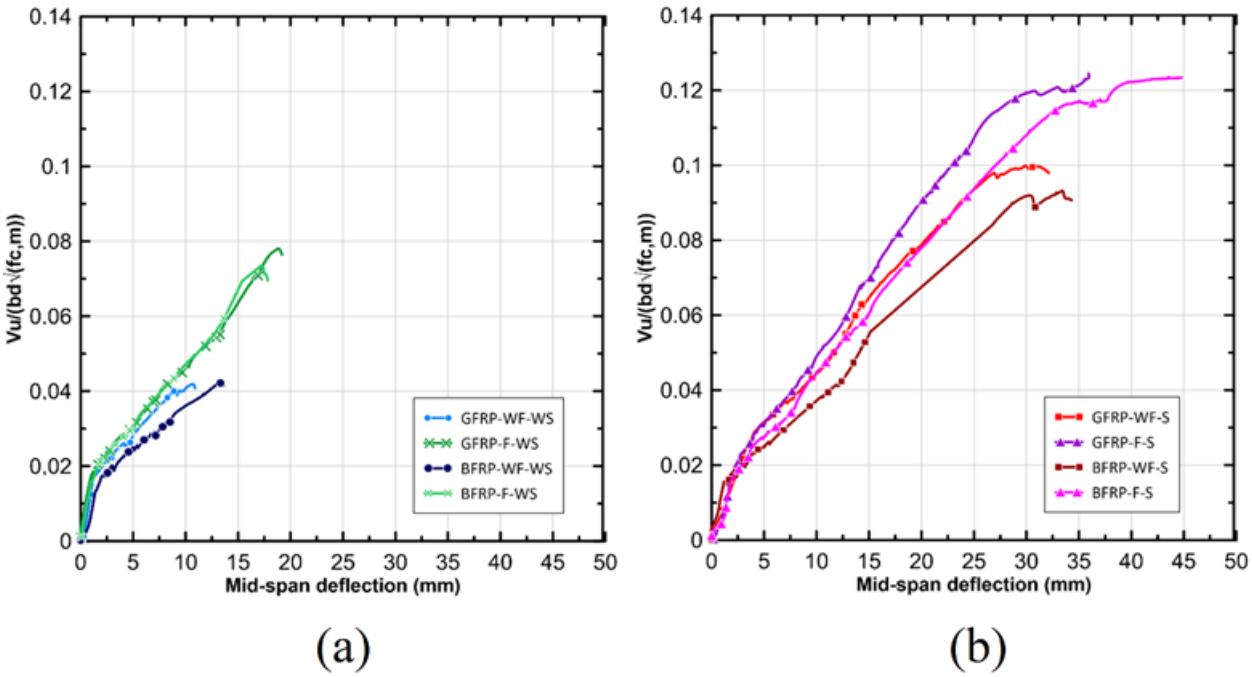

Figure 6. Experimental curves of normalized shear load × mid-span deflection of beams without stirrups (**a**) and with stirrups (**b**).

Table 6. Normalized shear resistance results.

ID	$f_{c,m}$ (MPa)	V_U Experimental (kN)	$\frac{V}{bd\sqrt{f_{c,m}}}$
GFRP-WF-WS	49.20	35.11	0.042
GFRP-WF-S	49.20	83.75	0.100
GFRP-F-WS	45.25	62.68	0.078
GFRP-F-S	45.25	100.01	0.124
BFRP-WF-WS	42.37	33.05	0.042
BFRP-WF-S	42.37	72.56	0.093
BFRP-F-WS	36.39	52.98	0.073
BFRP-F-S	36.39	89.08	0.124

3.1. Rebar Deformation

Strain gauges were installed in the longitudinal reinforcements (the two rebars of the extremities). The rebar strain was read and plotted against the applied load in Figure 7. All GFRP rebars showed the same behavior throughout the test. A first stage is observed, in which concrete is the main material responsible for resisting the loads. Then, when the load exceeds about 30 kN, the reinforcement is more requested. This is the expected behavior and was also observed by other works [33–38]. Initially, the curve presents a steep slope, representing the condition of sound concrete without cracks. At this point, the concrete is resisting tensile stresses. After cracking initiates, the resistant section of the concrete decreases, and the longitudinal bars are increasingly requested so that it is possible to observe a change in the slope of the curve. The curve remains linear until the structure ruptures. The BFRP rebar's behavior is similar. In the first stage, concrete is the main material responsible for resisting the loads. Then, when the load exceeds about 25 kN, the concrete begins to crack, and then the reinforcement is more requested, maintaining linear behavior until the end of the test.

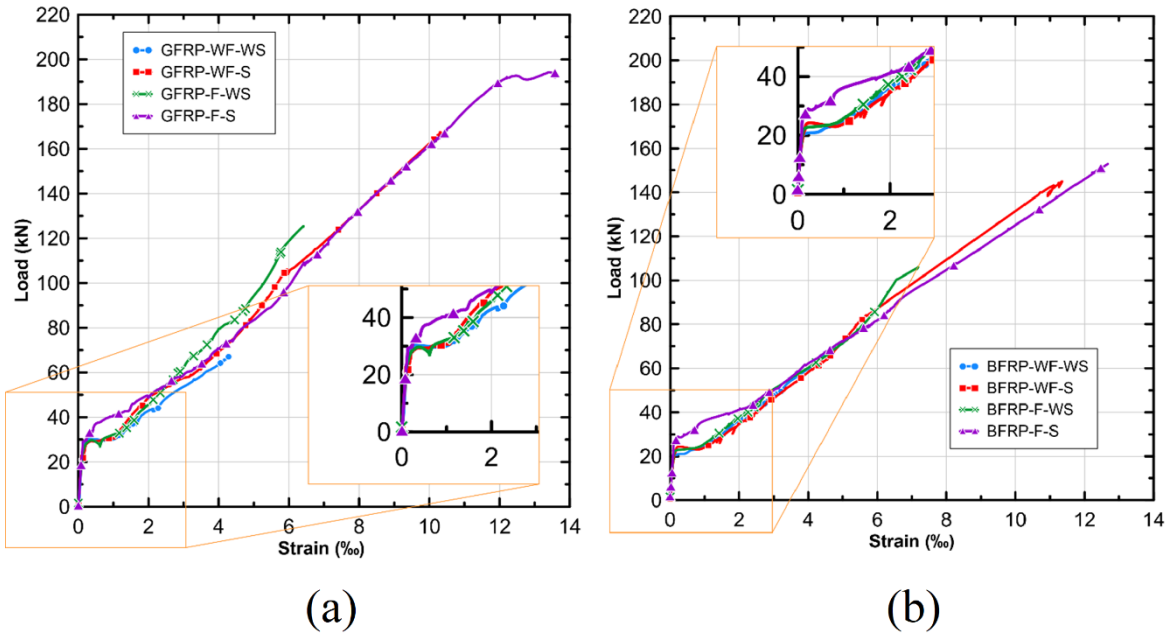

Figure 7. Load × specific deformation of longitudinal reinforcement of GFPR (**a**) and BFRP (**b**) beams.

3.2. Crack Openings

The curves of load × crack opening were obtained using digital image correlation analysis (Figure 3). Figure 8 presents the results of the beams. Observing the curves in Figure 8a, one may conclude that the addition of fibers and the presence of stirrups provided a reduction in the crack opening for the same load values. For example, for a

1 mm crack opening, the loads resisted by the beam with plain concrete GFRP-WF-WS increased from 32 kN to 50 kN due to the addition of fibers (GFRP-F-WS), an increment of 56%. The same is observed for beams GFRP-WF-S and GFRP-F-S; the load capacity increased from 57.5 kN to 76.5 kN, an increment of 33%, due to the addition of fibers. The presence of stirrups also increases the load for the same crack opening (1 mm). The comparison of beams GFRP-WF-WS and GFRP-WF-S shows an increase from 32 kN to 57.5 kN, an increment of 80%. Comparing the beams GFRP-F-WS and GFRP-F-S shows an increase from 50 kN to 76.5 kN, an increment of 53%.

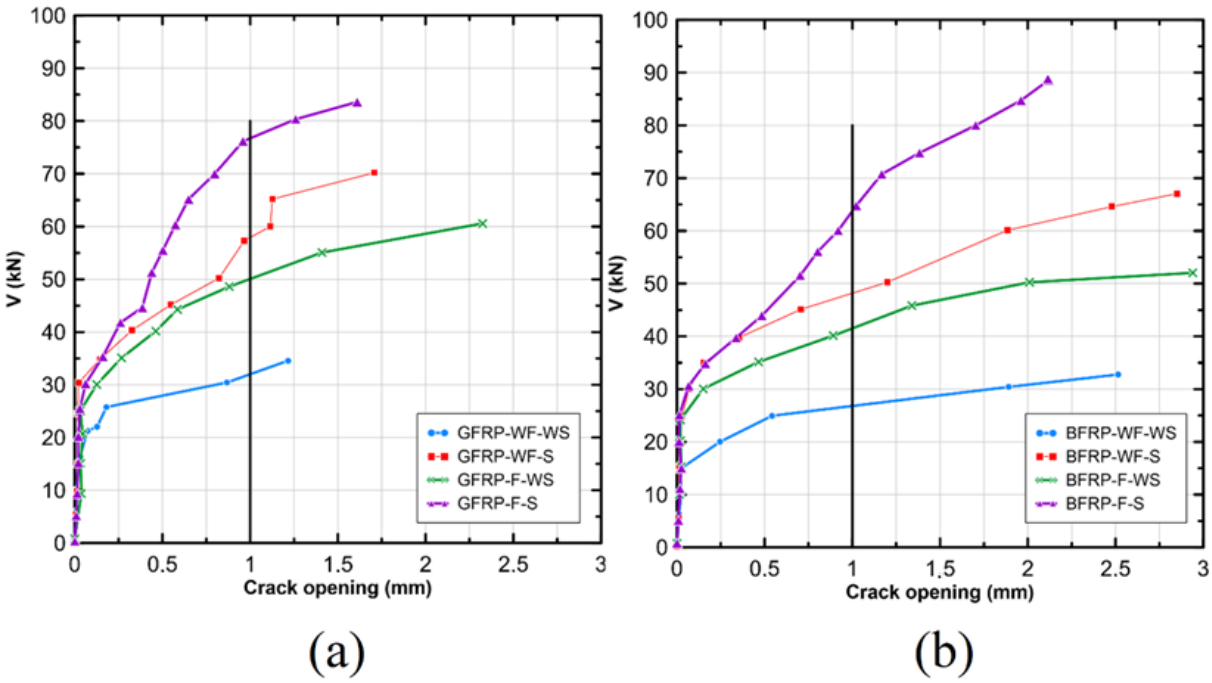

Figure 8. Shear load × crack opening curves for beams reinforced with GFRP (**a**) and BFRP (**b**) bars.

Similar behavior is observed for beams with BFRP rebars (Figure 8b). A clear reduction in crack openings is observed when the fiber is added to the concrete mix and in the presence of stirrups. For a crack opening of 1 mm, the addition of fibers promoted a load increase of 54% when comparing beams BFRP-WF-WS (27 kN) and BFRP-F-WS (41.5 kN) and a load increase of 32% when comparing beams BFRP-WF-S (48 kN) and BFRP-F-S (63.5 kN). The presence of stirrups promoted a load increase of 78% when comparing beams BFRP-WF-WS (27 kN) and BFRP-WF-S (48 kN) and a load increase of 53% when comparing beams BFRP-F-WS (41.5 kN) and BFRP-F-S (63.5 kN).

3.3. Analytical Calculations

This section describes the design of beams under flexure and shear loads. The ACI 440.1R-15 [17] standard is adopted to determine the moment and shear resistance of the beams with FRP rebars. Then, to account for the contribution of the macro fibers, Fib 2010 [18] is adopted.

3.3.1. Design of Beams According to ACI 440.1R-15 [17]

According to ACI 440.1R-15 [17], for flexural design, the parameters used to define the type of failure are the element's FRP reinforcement rate and the balanced reinforcement rate (reinforcement rate at which both types of failure—FRP rupture and concrete crushing—occur simultaneously).

The FRP reinforcement ratio (ρ_f) is defined by Equation (2), where A_f is the area of the FRP bars in mm^2, b is the width of the concrete beam in mm, and d is the useful height of the concrete beam, in mm.

$$\rho_f = \frac{A_f}{bd} \tag{2}$$

The balanced reinforcement ratio ρ_{fb} is given by Equation (3), where β_1 is a reduction factor, f'_c is the concrete's characteristic compressive strength, in MPa, E_f is the design modulus of elasticity of the FRP bar, f_{fu} is the calculated tensile strength of the FRP bar, and ε_{cu} is the ultimate strain of the concrete.

$$\rho_{fb} = 0.85 \cdot \frac{f'_c}{f_{fu}} \cdot \beta_1 \cdot \frac{E_f \cdot \varepsilon_{cu}}{E_f \cdot \varepsilon_{cu} + f_{fu}} \tag{3}$$

From Equation (4), f_{fu} is obtained, where $f^*_{fu} = f_{u,\,ave} - 3\sigma$, with $f_{u,\,ave}$ being the average tensile strength, σ the standard deviation, and C_E the coefficient of environmental reduction in the mechanical properties of fibers due to their exposure conditions ($C_E = 1$ was adopted).

$$f_{fu} = C_E f^*_{fu} \tag{4}$$

When $\rho_f > \rho_{fb}$, the failure of the structure is initiated by the crushing of the concrete. In this case, the stress in the FRP reinforcement f_f is given by Equation (5).

$$f_f = \left[\sqrt{\frac{\left(E_f \varepsilon_{cu}\right)^2}{4} + \frac{0.85 \beta_1 f_c{}'}{\rho_f} E_f \varepsilon_{cu}} - 0.5 E_f \varepsilon_{cu} \right] \leq f_{fu} \tag{5}$$

From the tension in the bar, it is possible to calculate the nominal resistant moment using Equation (6).

$$M_n = \rho_f f_f \left(1 - 0.59 \frac{\rho_f f_f}{f_c{}'}\right) bd^2 \tag{6}$$

When $\rho_f < \rho_{fb}$, the failure of the structure is governed by the rupture of the bar, thus the nominal resistant moment is calculated by Equation (7), where $c_b = \left(\frac{\varepsilon_{cu}}{\varepsilon_{cu} + \varepsilon_{fu}}\right) d$.

$$M_n = A_f f_{fu} \left(d - \frac{\beta_1 c_b}{2}\right) \tag{7}$$

According to ACI 440.1R-15 [17], the shear capacity of the concrete is given by Equation (8).

$$V_c = \frac{2}{5} \sqrt{f'_c}\, b_w (kd) \tag{8}$$

Here, $k = \sqrt{2\,\rho_f \eta_f + (\rho_f \eta_f)^2} - \rho_f \eta_f$, where k is the ratio of depth neutral axis to reinforcement depth, η_f is the ratio of Young's modulus of the FRP bars to Young's modulus of the concrete, f'_c is the specified compressive strength of the concrete, b_w is the width of the beam, and d is the distance from the extreme compression fiber to the centroid of tension reinforcement.

The contribution of the FRP stirrups positioned perpendicular to the element axis is given by Equation (9).

$$V_f = \frac{A_{fv}\, f_{fv}\, d}{s} \tag{9}$$

Here, A_{fv} (mm^2) is the amount of FRP shear reinforcement within spacing s, $f_{fv} = 0.004 E_f$, f_{fv} is the tensile strength of FRP for shear design, taken as the smallest of design tensile strength f_{fu}, the strength of the bent portion of FRP stirrups f_{fb}, or

the stress corresponding to $0.004E_f$, and E_f is the design modulus of elasticity of the FRP bar.

3.3.2. Ultimate Limit State Design of Linear Elements with Fiber-Reinforced Concrete (FRC) Subjected to Shear Force—Fib 2010 [18]

According to Fib 2010 [17], the bending failure stage is supposed to be reached when one of the following conditions applies: attainment of the ultimate compressive strain in the fiber-reinforced concrete (FRC), ε_{cu}; attainment of the ultimate tensile strain in the steel (if present), ε_{su}; and attainment of the ultimate tensile strain in the FRC, ε_{Fu}.

When using the FRC in structural elements without transverse reinforcement, the element strength at a given cross section is calculated according to Equation (10).

$$V_{Rd,F} = \left\{ \frac{0.18}{\gamma_c} k \left[100\,\rho_1 \left(1 + 7.5 \frac{f_{Ftuk}}{f_{ctk}} \right) f_{ck} \right]^{\frac{1}{3}} + 0.15\sigma_{cp} \right\} b_w d \quad (10)$$

Here, γ_c is the weighting coefficient of FRC; d is the distance from the extreme compression fiber to the centroid of tension reinforcement, in mm; b_w is the width of the beam, in mm; f_{Ftuk} is the characteristic strength to the direct traction of FRC, the ultimate value, considering $w_u = 1.5$ mm, in MPa; f_{ctk} is the characteristic strength of the concrete to the direct traction, expressed in MPa; f_{ck} is the characteristic compressive strength of concrete, in MPa; and $k = 1 + \sqrt{\frac{200}{d}} \leq 2.0$; $\rho_1 = \frac{A_{sl}}{(b_w d)}$, where ρ_1 is the longitudinal reinforcement ratio and A_{sl} is the cross-sectional area of the reinforcement; $\sigma_{cp} = \frac{N_{Ed}}{A_c} \leq 0.2 f_{cd}$, where σ_{cp} is the average stress in the concrete cross section (A_c) by axial force action (N_{Ed}) due to loading or prestressing actions ($N_{Ed} > 0$ for compression).

3.3.3. Comparison between Theoretical and Experimental Results

The analytical calculations are compared to the experimental results. Table 7 shows the resistant moment calculated based on ACI 440.1R-15 [17] and Fib 2010 [18]. Then, these two values are simply added and compared to the experimental results with great agreement.

Table 7. A comparison of the experimental results and the calculation of flexural resistance based on ACI 440.1R-15 [17] and Fib 2010 [18].

ID	ACI 440.1R-15 [17]	Fib 2010 [18]	Mn (kN·m)	$M_{u,exp}$ (kN·m)	$M_{u,exp}/M_n$
	Mn (kN·m)	Mn (kN·m)			
GFRP-F-S	54.37	8.73	63.10	62.66	0.99
BFRP-F-S	48.61	7.15	55.76	56.13	1.01

The calculations of flexural resistance according to ACI 440.1R-15 [17] were performed considering the reinforcement arrangements adopted and the average values of the properties of the bars and concrete, as obtained in the characterization of the materials. The analysis addressed only the GFRP-F-S and BFRP-F-S beams, which were the two that exhibited flexural failure. For the calculation of the fiber-reinforced concrete's contribution to the beam's resistant moment, an approach based on the Fib 2010 standard [18] was adopted, through stress equilibrium. From the neutral line obtained from the design of FRP-reinforced beams, according to ACI 440.1R-15 [17], the section of the beam subjected to tension was calculated, which, multiplied by the direct tensile strength of the FRC and the distance in relation to the center of the compressed section, resulted in the resistant portion of the fiber-reinforced concrete.

Table 8 shows the shear resistance calculated according to ACI 440.1R-15 [17] and according to Fib 2010 [18]. The shear resistance is given by the contribution of the concrete and the stirrups (when they exist). It is proposed to calculate the contribution of the concrete section either with ACI 440.1R-15 [17] or Fib 2010 [18]. The beams with the addition of

macro fibers are calculated using Fib 2010 [18], and the beams with plain concrete are calculated using ACI 440.1R-15 [17]. The calculations of shear resistance according to ACI 440.1R-15 [17] were performed considering the reinforcement arrangements adopted (stirrups spaced at 21 cm) and the average values of the properties of the bars and concrete obtained in the characterization of the materials. Beams GFRP-F-S and BFRP-F-S exhibited flexural failure in the tests. Therefore, their experimental shear load does not represent its full shear capacity.

Table 8. A comparison of the experimental results and the calculation of shear resistance according to ACI 440.1R-15 [17] and Fib 2010 [18].

ID	ACI 440.1R-15 [17]		Fib 2010 [18]	V_v (kN)	$V_{u,exp}$	$V_{u,exp}/V_n$
	V_C (kN)	V_f (kN)	$V_{Rd,F}$ (kN)			
GFRP-WF-WS	18.92	-	-	18.92	35.11	1.86
GFRP-WF-S	18.92	23.25	-	42.17	83.75	1.99
GFRP-F-WS	-	-	75.49	75.49	62.68	0.83
GFRP-F-S	-	23.25	75.49	98.74	99.46	1.00
BFRP-WF-WS	17.28	-	-	17.28	33.04	1.91
BFRP-WF-S	17.28	23.99	-	41.27	72.55	1.76
BFRP-F-WS	-	-	65.37	65.37	52.99	0.81
BFRP-F-S	-	23.99	65.37	89.36	89.10	1.00

It is possible to observe that the shear resistance calculated by ACI 440.1R-15 [17] underestimated both the contribution of concrete, V_c, and the contribution of stirrups, V_f. The largest difference found between the theoretical and experimental calculations was for the beam reinforced with GFRP bars and stirrups (a ratio of 1.99).

When analyzing the $V_{rd,f}$, according to Fib 2010 [18], it is noted that the theoretical calculation overestimated the contribution of concrete with fiber, since the experimental results represented 83% and 81% of the theoretical value, for the beams reinforced with GFRP and BFRP bars, respectively.

4. Conclusions

This work assessed the contribution of macro fiber addition in the shear resistance of concrete beams with FRP rebars. The experimental study analyzed the partial and total replacement of FRP stirrups by polymeric macro fiber in the content of 1% in concrete volume, in reinforced concrete beams with GFRP and BFRP rebars. From the results, the following conclusions can be drawn:

- The total replacement of GFRP and BFRP stirrups with polypropylene macro fibers did not prevent brittle shear failure.
- The addition of macro fibers enhanced the shear resistance. The results showed increases of 78.5% for the beams with GFRP rebars and 60.4% for the beams with BFRP.
- The addition of macro fibers in the beams with insufficient stirrups, i.e., with excessive spacing, changed the failure mode from brittle shear failure to pseudo-ductile flexural failure due to concrete crushing. In these cases, the failure load increased by 18.8% for beams with GFRP bars and 22.8% for beams with BFRP bars.
- The analysis of mid-span deflection indicates that beams with insufficient stirrups improved their ductility when macro fibers were added.
- The addition of fibers in the concrete mix reduced crack openings. The comparison of shear load for the same crack opening indicated an increase of up to 56%. In the presence of stirrups, fibers promoted a higher contribution, with an increase in load capacity for the same crack opening of up to 80%.
- An analytical calculation of the nominal moment resistance, based on the procedures of ACI 440.1R-15 [17] and Fib 2010 [18], for the two beams that exhibited flexural failure

resulted in values very close to the experimental one (a ratio of 0.99 for GFRP-F-S and 1.01 for BFRP-F-S).

- The beam's shear resistance calculated by ACI 440.1R-15 [17] underestimated both the contribution of concrete and the contribution of stirrups when compared to the experimental results. The most significant discrepancy between theoretical and experimental values occurred in the beam reinforced with GFRP bars and stirrups, exhibiting a ratio of 1.99.
- When analyzing the shear resistance of the fiber-reinforced concrete according to Fib 2010 [18], it is noted that the theoretical calculation overestimated the contribution of concrete with fiber, since the experimental result represented 83% and 81% of the theoretical value, for the beams with GFRP and BFRP rebars, respectively.

Author Contributions: I.O.D.: conceptualization, data curation, data analysis, methodology, writing; N.C.d.S.F.: conceptualization, formal analysis, supervision, writing, resources, funding acquisition; L.L.P.: methodology, supervision, formal analysis; A.E.P.G.d.A.J.: methodology, supervision, formal analysis. All authors have read and agreed to the published version of the manuscript.

Funding: This research was funded by Haizer Group grant number PUC 5246.

Data Availability Statement: The raw data supporting the conclusions of this article will be made available by the authors on request.

Acknowledgments: We would like to express gratitude to the Haizer Group company for the supply of materials for the execution of the research and the scholarship.

Conflicts of Interest: The authors declare no conflicts of interest.

References

1. de Sá, F.R.; Silva, F.D.A.; Cardoso, D.C. Tensile and flexural performance of concrete members reinforced with polypropylene fibers and GFRP bars. *Compos. Struct.* **2020**, *253*, 112784. [CrossRef]
2. Younis, A.; Ebead, U.; Judd, S. Life cycle cost analysis of structural concrete using seawater, recycled concrete aggregate, and GFRP reinforcement. *Constr. Build. Mater.* **2018**, *175*, 152–160. [CrossRef]
3. Imjai, T.; Garcia, R.; Kim, B.; Hansapinyo, C.; Sukontasukkul, P. Serviceability behaviour of FRP-reinforced slatted slabs made of high-content recycled aggregate concrete. *Structures* **2023**, *51*, 1071–1082. [CrossRef]
4. Reis, V.L.F. Construction of Concrete Structures Reinforced with FRP Rods. Master's Thesis, University of Porto, Porto, Portugal, 2009.
5. Yang, Y.; Liu, G. Data-Driven Shear Strength Prediction of FRP-Reinforced Concrete Beams without Stirrups Based on Machine Learning Methods. *Buildings* **2023**, *13*, 313. [CrossRef]
6. El-Sayed, A.K.; El-Salakawy, E.F.; Benmokrane, B. Shear capacity of high-strength concrete beams reinforced with FRP bars. *ACI Struct. J.* **2006**, *103*, 383–389. [CrossRef]
7. Razaqpur, A.G.; Isgor, O.B. Proposed shear design method for FRP-reinforced concrete members without stirrups. *ACI Struct. J.* **2006**, *103*, 93–102. [CrossRef]
8. Gomes, T.A.; Resende, T.M.; Cardoso, D.C.T. Shear-transfer mechanisms in reinforced concrete beams with GFRP bars and basalt fibers. *Eng. Struct.* **2023**, *289*, 116299. [CrossRef]
9. Kassem, C.; Farghaly, A.S.; Benmokrane, B. Evaluation of flexural behavior and serviceability performance of concrete beams reinforced with FRP bars. *J. Compos. Constr.* **2011**, *15*, 682–695. [CrossRef]
10. Adam, M.A.; Said, M.; Mahmoud, A.A.; Shanour, A.S. Analytical and experimental flexural behavior of concrete beams reinforced with glass fiber reinforced polymers bars. *Constr. Build. Mater.* **2015**, *84*, 354–366. [CrossRef]
11. Awadallah, Z.H.; Ahmed, M.M.; Farghal, O.A.; Fahmy, M.F.M. Some Parameters Affecting Shear Behavior of High Strength Fiber Reinforced Concrete Beams Longitudinally Reinforced With BFRP Rebars. *JES. J. Eng. Sci.* **2014**, *42*, 1163–1178. [CrossRef]
12. Muhammad, J.H.; Yousif, A.R. Shear behavior of normal and high-strength concrete beams reinforced with BFRP bars and basalt macro fibers. *Constr. Build. Mater.* **2023**, *408*, 133516. [CrossRef]
13. Dev, A.; Chellapandian, M.; Prakash, S.S. Effect of Macrosynthetic and Hybrid Fibers on Shear Behavior of Concrete Beams Reinforced with GFRP Bars. *J. Bridge Eng.* **2020**, *25*, 04020031. [CrossRef]
14. Tapkın, S. The effect of polypropylene fibers on asphalt performance. *Build. Environ.* **2008**, *43*, 1065–1071. [CrossRef]
15. Behfarnia, K.; Behravan, A. Application of high performance polypropylene fiber in concrete lining of water tunnels. *Mater. Des.* **2014**, *55*, 274–279. [CrossRef]
16. Cardoso, D.C.; Pereira, G.B.; Silva, F.A.; Silva Filho, J.J.; Pereira, E.V. Influence of steel fibers on the flexural behavior of RC beams with low reinforcing ratios: Analytical and experimental investigation. *Compos. Struct.* **2019**, *222*, 110926. [CrossRef]

17. *ACI 440. 1R–15*; Guide for the Design and Construction of Structural Concrete Reinforced with Fiber-Reinforced Polymer (FRP) Bars. ACI Committee 440; American Concrete Institute: Farmington Hills, MI, USA, 2015.
18. International Federation for Structural Concrete (fib). *Fib Model Code for Concrete Structures 2010*; International Federation for Structural Concrete (fib): Lausanne, Switzerland, 2010.
19. *NBR 7211-2019*; Aggregates for Concrete—Specification. Brazilian Association of Technical Standards (ABNT): Rio de Janeiro, Brazil, 2019.
20. *NBR 16916-2021*; Fine Aggregate—Determination of Water Density and Absorption. Brazilian Association of Technical Standards (ABNT): Rio de Janeiro, Brazil, 2021.
21. *NBR 16917-2021*; Coarse Aggregate—Determination of Water Density and Absorption. Brazilian Association of Technical Standards (ABNT): Rio de Janeiro, Brazil, 2021.
22. *EN 14889-2:2008*; Fibres for Concrete—Part 2: Polymer Fibres—Definitions, Specifications and Conformity. European Committee for Standardization: Brussels, Belgium, 2008.
23. *NBR 16889-2020*; Concrete-Determination of Consistency by Slump Test. Brazilian Association of Technical Standards (ABNT): Rio de Janeiro, Brazil, 2020.
24. *NBR 5739-2018*; Concrete-Cylindrical Specimen Compression Test. Brazilian Association of Technical Standards (ABNT): Rio de Janeiro, Brazil, 2018.
25. *NBR 12142-2010*; Concrete-Determination of Tensile Strength in the Bending of Prismatic Specimens. Brazilian Association of Technical Standards (ABNT): Rio de Janeiro, Brazil, 2010.
26. *NBR 8522-2017*; Concrete—Determination of Static Modules of Elasticity and Deformation to Compression. Brazilian Association of Technical Standards (ABNT): Rio de Janeiro, Brazil, 2017.
27. *NBR 16940-2021*; Fiber Reinforced Concrete-Determination of Tensile Strengths in Bending (Proportionality Limit and Residual Resistances)—Test Method. Brazilian Association of Technical Standards (ABNT): Rio de Janeiro, Brazil, 2021.
28. *ASTMD7205/D7205-M-21*; Standard Test Method for Tensile Properties of Fiber Reinforced Polymer Matrix Composite Bars. ASTM International: West Conshohocken, PA, USA, 2021.
29. Bhosale, A.B.; Prakash, S.S. Crack Propagation Analysis of Synthetic vs. Steel vs. Hybrid Fibre-Reinforced Concrete Beams Using Digital Image Correlation Technique. *Int. J. Concr. Struct. Mater.* **2020**, *14*, 57. [CrossRef]
30. Lecompte, D.; Smits, A.; Bossuyt, S.; Sol, H.; Vantomme, J.; Van Hemelrijck, D.; Habraken, A. Quality assessment of speckle patterns for digital image correlation. *Opt. Lasers Eng.* **2006**, *44*, 1132–1145. [CrossRef]
31. Imjai, T.; Kefyalew, F.; Aosai, P.; Garcia, R.; Kim, B. A new equation to predict the shear strength of recycled aggregate concrete Z puch-off specimens. *Cem. Concr. Res.* **2023**, *169*, 107181. [CrossRef]
32. *GOM Software*, V2.0.1. 2018. Available online: https://www.zeiss.com/metrology/en/software/metrology-software.html (accessed on 16 May 2024).
33. Said, M.; Adam, M.A.; Mahmoud, A.A.; Shanour, A.S. Experimental and analytical shear evaluation of concrete beams reinforced with glass fiber reinforced polymers bars. *Constr. Build. Mater.* **2016**, *102*, 574–591. [CrossRef]
34. Tomlinson, D.; Fam, A. Performance of concrete beams reinforced with basalt FRP for flexure and shear. *J. Compos. Constr.* **2014**, *19*, 04014036. [CrossRef]
35. Abed, F.; Alhafiz, A.R. Effect of basalt fibers on the flexural behavior of concrete beams reinforced with BFRP bars. *Compos. Struct.* **2019**, *215*, 23–34. [CrossRef]
36. Huang, Z.; Chen, W.; Hao, H.; Chen, Z.; Pham, T.M.; Tran, T.T.; Elchalakani, M. Shear behaviour of ambient cured geopolymer concrete beams reinforced with BFRP bars under static and impact loads. *Eng. Struct.* **2021**, *231*, 111730. [CrossRef]
37. Junaid, M.T.; Elbana, A.; Altoubat, S.; Al-Sadoon, Z. Experimental study on the effect of matrix on the flexural behavior of beams reinforced with Glass Fiber Reinforced Polymer (GFRP) bars. *Compos. Struct.* **2019**, *222*, 110930. [CrossRef]
38. El-Nemr, A.; Ahmed, E.A.; El-Safty, A.; Benmokrane, B. Evaluation of the flexural strength and serviceability of concrete beams reinforced with different types of GFRP bars. *Eng. Struct.* **2018**, *173*, 606–619. [CrossRef]

Disclaimer/Publisher's Note: The statements, opinions and data contained in all publications are solely those of the individual author(s) and contributor(s) and not of MDPI and/or the editor(s). MDPI and/or the editor(s) disclaim responsibility for any injury to people or property resulting from any ideas, methods, instructions or products referred to in the content.